Some characteristics of intense geomagnetic storms and their energy budget

Geeta Vichare,[1] S. Alex, and G. S. Lakhina
Indian Institute of Geomagnetism, Navi Mumbai, India

Received 4 February 2004; revised 23 November 2004; accepted 8 December 2004; published 4 March 2005.

[1] The present study analyses nine intense geomagnetic storms ($|Dst| > 175$ nT) with the aid of ACE satellite measurements and ground magnetic field values at Alibag Magnetic Observatory. The study confirms the crucial role of southward IMF in triggering the storm main phase as well as controlling the magnitude of the storm. The main phase interval shows clear dependence on the duration of southward IMF. An attempt is made to identify the multipeak signature in the ring current energy injection rate during main phase of the storm. In order to quantify the energy budget of magnetic storms, the present paper computes the solar wind energies, magnetospheric coupling energies, auroral and Joule heating energies, and the ring current energies for each storm under examination. Computation of the solar wind- magnetosphere coupling function considers the variation of the size of the magnetosphere by using the measured solar wind ram pressure. During the main phase of the storm, the solar wind kinetic energy ranges from 9×10^{17} to 72×10^{17} J with an average of 30×10^{17} J; the total energy dissipated in the auroral ionosphere varies between 2×10^{15} and 9×10^{15} J, whereas ring current energies range from 8×10^{15} to 19×10^{15} J. For the total storm period, about 3.5% of total solar wind kinetic energy is available for the redistribution in the magnetosphere, and around 20% of this goes into the inner magnetosphere and in the auroral ionosphere of both the hemispheres. It is found that during main phase of the storm, almost 5% of the total solar wind kinetic energy is available for the redistribution in the magnetosphere, whereas during the recovery phase the percentage becomes 2.3%.

Citation: Vichare, G., S. Alex, and G. S. Lakhina (2005), Some characteristics of intense geomagnetic storms and their energy budget, *J. Geophys. Res.*, *110*, A03204, doi:10.1029/2004JA010418.

1. Introduction

[2] Understanding geomagnetic storms in terms of energies involved in various associated processes has been a longstanding problem. Availability of satellite measurements of various interplanetary plasma and magnetic field parameters associated with the development of geomagnetic storms has provided a unique platform for investigating the interplanetary causes of geomagnetic storms [*Tsurutani and Gonzalez*, 1997; *Huttunen et al.*, 2002; *Turner et al.*, 2001]. Besides these observational studies, the problem has been tackled through modeling studies [*Feldstein*, 1992; *Alexeev and Feldstein*, 2001], and using simulation analysis [*Ebihara and Ejiri*, 2000] as well. Nevertheless, a variety of storm mechanisms have been reported [*Gonzalez et al.*, 2001] due to the complexity involved in each storm event. This complexity could be due to varying nature of the storm sources such as simple coronal mass ejections (CMEs), magnetic cloud structures, multiple occurrences of CMEs, high-speed solar wind streams, etc. The magnetosphere responds differently to different interplanetary causes, thus leading to the alteration of the energy budget involved in each storm. Under these circumstances it is necessary to perform detailed qualitative and quantitative study of the storm time energetics of large number of storms. This could provide deeper insight into the better description of the phenomenon.

[3] We have analyzed intense magnetic storms for the period between 1998 and 2001, which covers part of ascending and descending phases of the solar cycle near solar maximum. Sections 2 and 3 discuss about the data selection and the energetics of the solar wind, respectively. Case study of few representative storm events is done in section 4, whereas section 5 demonstrates magnetic cloud situation. Results of present investigation including statistical analysis and quantitative assessment of the energy budget involved in each case are sketched out in section 6. Section 7 brings out the summary of the paper.

2. Data Selection and Method of Analysis

[4] The disturbance storm time (*Dst*) index is a measure of geomagnetic activity, and has been commonly used to assess the strength of geomagnetic storms [*Yokoyama and Kamide*, 1997]. According to some researchers, the condi-

[1] Formerly Geeta Jadhav.

0148-0227/05/2004JA010418$09.00

tion that leads to the development of the ring current is due to the successive occurrence of many substorms, which are measured by the *AE* index [*Akasofu and Chapman*, 1961; *Chapman*, 1962]. At the same time, some believe that a fluctuating interplanetary magnetic field (IMF), even with smaller southward amplitude, could result in enhanced *AE* but not in larger deviation of *Dst* index [*Garrett et al.*, 1974]. A recent paper by *Kamide* [2001] states that the steady southward IMF is important in the formation of magnetic storm, while fluctuations in the solar wind electric fields are responsible for initiating magnetospheric substorms. During magnetic storms, auroral electrojet shifts equatorward. Hence the *AE* indices based on subauroral observatories are more relevant for the magnetic storm studies. However, the *AE* indices of 1-min time resolution used in the present study are downloaded from World Data Center, Kyoto, which are based on maximum of 12 auroral observatories (geomagnetic latitude > 60°).

[5] In the case of a classic magnetic storm, the *Dst* shows a sudden rise, corresponding to the storm sudden commencement, and then decreases sharply as the ring current intensifies; IMF is southward during this time interval. Once the IMF turns northward again and the ring current begins to recover, the *Dst* begins to rise slowly back to its quiet time level. The relationship of inverse proportionality between the decrease of the horizontal component of the magnetic field and the energy content of the ring current is known as the Dessler-Parker-Sckopke (DPS) relation [*Dessler and Parker*, 1959; *Sckopke*, 1966]. Other currents contribute to the *Dst* as well, most importantly the magnetopause current. Hence the *Dst* indices are corrected to remove the contribution of this current and that of the quiet time ring current.

[6] We have identified nine intense magnetic storms ($|Dst| > 175$ nT), for the period from 1998 to 2001, with the help of hourly values of *Dst* index provided by Kyoto World Data Center (see Table 1). Identification of these storms is done irrespective of the presence of the initial phase [*Joselyn and Tsurutani*, 1990]. Since magnetopause currents can also contribute to the field perturbations felt on the Earth, we correct *Dst* values for solar wind ram pressure [*Burton et al.*, 1975],

$$Dst^* = Dst - b \cdot P^{1/2} + c, \quad (1)$$

where P is solar wind dynamic pressure, and the coefficients are set to $b = 8.74$ nT $(\text{nPa})^{-1/2}$ and $c = 11.54$ nT [*Turner et al.*, 2001].

[7] Further, to study the effect of intense storm on the low-latitude magnetic field, we have used the horizontal magnetic field variation data with 1-min time resolution from Alibag Magnetic Observatory operated by the Indian Institute of Geomagnetism (IIG), Mumbai.

[8] The solar wind parameters such as wind velocity, density, temperature, and IMF components obtained from ACE satellite measurements are downloaded from the Internet (http://nssdc.gsfc.nasa.gov). The solar wind data is based on Solar Wind Electron Proton Alpha Monitor (SWEPAM) measurements, while IMF data is obtained from ACE Magnetic Field Instrument. These measurements with sampling rate of 0.003 Hz are obtained for GSM coordinate system. Thus we get data set of solar wind

Table 1. Intense Geomagnetic Storm Events

Storm	Date	Dst* Min, nT	Time Delay for Shock to Get Recorded at Ground Station, min	Main Phase Duration, hour	B_z Magnitude of Max Southward IMF, nT	Duration of Southward IMF, hr	Multiple Peak Structure	Comment
1	4 May 98	−230	30	2	36	2.3	No	No initial phase
2	25 Sep 98	−206	35	9	22.7	14	Yes	Magnetic cloud
3	22 Sep 99	−178	30	3	22	4.4	No	Long initial phase (~7 hours)
4	22 Oct 99	−266	60	7	31.5	8	Yes	SSC is seen ~22 hours before storm development. Magnetic cloud?
5	6 Apr 00	−314	38	7	33.3	9	Yes	Magnetic cloud
6	12 Aug 00	−239	No SSC	8	30	15	Yes	Magnetic cloud
7	17 Sep 00	−226	No SSC	4	32.6	4.2	No	Disturbed before onset of the storm
8	31 Mar 01	−381	35	5	47	4	No	Two-step storm
9	11 Apr 01	−259	40	9	32	8	Yes	Magnetic cloud

parameters and IMF in GSM coordinates with 5-min time resolution. We next calculate solar wind pressure (SW_{press}) and thermal pressure for the above data set.

[9] In the present study, we have analyzed nine intense storms in detail and their characteristics, which include maximum *Dst* deviation, time delay for shock to get recorded at ground station through the occurrence of SSC, main phase duration, maximum magnitude of southward IMF, and duration of southward IMF are given in Table 1.

[10] We have introduced an additional column to indicate whether the ring current energy injection rate exhibits the multipeak structure. The last column therein comments on some specific characteristics observed for a given storm event. The minimum value of *Dst* (pressure-corrected) for each storm event is the largest deviation of *Dst* from the zero level. In rest of the paper we deal with pressure-corrected *Dst* values only. It is known that the main phase starts with a rapid decrease of *Dst* and ends at the time of minimum *Dst* value [*Jacobs*, 1991], and hence the main phase duration in Table 1 indicates the time interval between these two. The SSC is recorded as a sudden rise in the low-latitude horizontal magnetic field component, with quiet background. The time delay between the shock seen by spacecraft at Lagrangian point (L1) and ground station depends on the solar wind speed. Approximately for the solar wind velocity of 350 km/s, time lag observed is ~60 min. In the present investigation, two events have been recorded without the occurrence of SSC. For 17 September 2000 storm, it was not possible to record SSC, maybe due to disturbed nature of the field variations ($Ap > 30$) before the onset of the storm event. The situation of magnetic cloud has been discussed later in more detail (see section 5). We will discuss the table as the study proceeds.

3. Energetics of the Solar Wind and Magnetosphere

[11] The kinetic energy of the interplanetary solar wind impinging on the magnetosphere per unit time can be given as

$$U_{SW} = (1/2) \cdot \rho \cdot V_{sw}^3 \cdot A, \quad (2)$$

where V_{sw} is solar wind velocity, ρ is mass density of solar wind, and A is the cross section of the dayside magnetosphere and is taken as $(30\ R_E)^2$ [*Weiss et al.*, 1992]. The solar wind-magnetosphere coupling parameters have been studied for several years [*Nishida*, 1983]. The most widely used coupling parameter is given by *Perreault and Akasofu* [1978] as

$$\text{Energy coupling function } \varepsilon = V_{sw} B^2 L_0^2 (\sin^4 \theta/2), \quad (3)$$

where B is the magnitude of the IMF, θ is the angle between the geomagnetic field vector and the IMF vector at the front of the magnetosphere in the equatorial plane, and L_0 is the radius of the dayside magnetopause. This expression shows that even under weakly northward IMF conditions, still significant energy coupling is possible.

[12] Normally, L_0 is considered to be fixed at 7 R_E, under the assumption of stationary dayside magnetopause

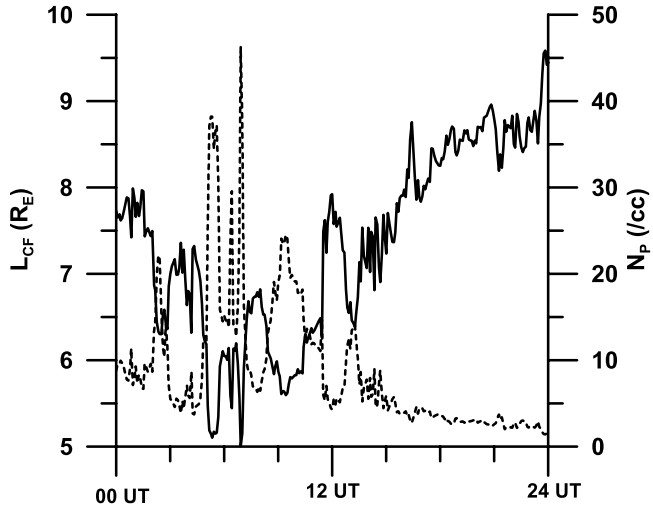

Figure 1. Variation of magnetopause boundary (solid line) on 4 May 1998. Solar wind proton number density variations are shown by dotted curve.

[*Perreault and Akasofu*, 1978; *Baker et al.*, 2001]. However, the solar wind dynamic pressure plays most important role in determining the position of the subsolar point [*Martyn*, 1951]. Therefore in practice, due to varying nature of solar wind pressure, the magnetopause does not remain stationary. The variation in the magnetopause boundary can be taken into account by considering Chapman-Ferraro magnetopause distance (L_{CF}), which is obtained from the balance between the kinetic plasma pressure and the magnetic pressure [*Sibeck et al.*, 1991; *MacMahon and Gonzalez*, 1997],

$$L_{CF} = \left(B_0^2/4\pi N m_p V_{sw}^2\right)^{1/6} R_E, \quad (4)$$

where B_0 is the Earth's magnetic field strength and R_E is the Earth's radius, whereas N and m_p represent the proton number density and proton mass, respectively. Using satellite data for magnetopause crossings, *Sibeck et al.* [1991] have verified the pressure balance relationship between the solar wind dynamic pressure and the location of the subsolar magnetopause.

[13] Figure 1 shows the variation of the magnetopause boundary (solid curve) calculated from equation (4) using ACE data, on 4 May 1998, along with the solar wind density variations shown by dotted curve. We observe a sudden increase in the solar density variations maximizing at 0230 UT, when magnetosphere boundary gets compressed to 6.5 R_E. We would like to point out that the proton monitor on SOHO satellite recorded the shock at 0210 UT, which is in agreement with the present ACE data based computations. Next higher density impulse with magnitude ~45/cc arrived around 0715 UT, during which boundary moved further inward to 5 R_E. This indicates that under some circumstances, around 30% of deviation could be observed in the magnetopause boundary distance, which could further alter the epsilon parameter significantly.

[14] *Akasofu* [1981a] gave a quantitative estimation of the total magnetospheric energy consumption rate, by assuming that the total energy contains major contribution from three components, namely, Joule heating rate (U_J), auroral parti-

cle energy precipitation rate (U_A), and ring current energy injection rate (U_{RC}). Therefore

$$U_T = U_J + U_A + U_{RC}. \quad (5)$$

Akasofu [1981a] approximated the terms U_J and U_A by the following relationship to the *AE* index

$$U_J = 2 \times 10^8 \text{ AE} \quad (6)$$

$$U_A = 1 \times 10^8 \text{ AE}, \quad (7)$$

where *AE* is in nT and dissipation power is in Watts.

[15] Later work by *Baumjohann and Kamide* [1984] has suggested that the Joule heating is actually much higher than that quantified by *Akasofu* [1981a]. They proposed $U_J = 3.2 \times 10^8$ AE. However, we use equation (6) for the calculation of U_J in the present investigation.

[16] Combining the energy balance equation with DPS relationship, the ring current injection rate can be obtained as

$$U_{RC} = -(3/2)(E_m/B_0)(dDst/dt + Dst/\tau), \quad (8)$$

where $E_m = 8 \times 10^{17}$ J is the total magnetic energy of the geomagnetic field outside the Earth, B_0 is strength of geomagnetic field at the equatorial surface, and τ is the decay time constant. The time variation of *Dst* index is proportional to the energy storage rate in the ring current, whereas second term describes the energy dissipation from the ring current, which is caused by various processes [*Liemohn et al.*, 1999; *Ebihara and Ejiri*, 2000]. The sign of first term (*dDst*/*dt*) indicates whether energy is stored (negative) or dissipated (positive).

[17] The ring current particle loss rate depends upon the particle species, energy, pitch angle, and *L* value. It is obvious that the value of τ is changing continuously during the magnetic storm. Satellite measurements show that during intense storms, ring current composition is significantly dominated by O^+ ions [*Hamilton et al.*, 1988], which have a much shorter lifetime to charge exchange than H^+ ions, that are usually the dominant contribution to the ring current. For practical purposes, the loss rate parameter τ is therefore an average over the whole ring. *MacMahon and Gonzalez* [1997] suggested that the decay time varies as $(Dst)^{-3/2}$, whereas *Valdivia et al.* [1996] proposed another function as τ = 12.5/(1-0.0012 *Dst*). An empirical analysis of *Dst* ring current by *O'Brien and McPherron* [2000] found that the ring current decay lifetime varies with the interplanetary electric field, $V_{sw}B_z$ but not with *Dst*, this could be due to the variation in the position of convection boundaries in the magnetosphere. However, we shall not attempt this here. Rather, we will use constant value of τ as 8 hours for intense geomagnetic storms [*Yokoyama and Kamide*, 1997].

4. Case Study

[18] Here we present case studies of only three storms as representative of the set.

4.1. The 22 October 1999 Storm

[19] Figure 2 draws synoptic picture of the geomagnetic activity taking place between 0000 UT on 21 October and 1900 UT on 22 October 1999. Various plots in this figure show 1-min values of horizontal magnetic field variations at Alibag (GMlat = 9°N) observatory, hourly averaged values of *Dst*, *AE* indices with 1-min time resolution, solar wind speed, density variations, and north-south component of interplanetary magnetic field. It also indicates solar wind particle-pressure, thermal pressure, and magnetospheric coupling function.

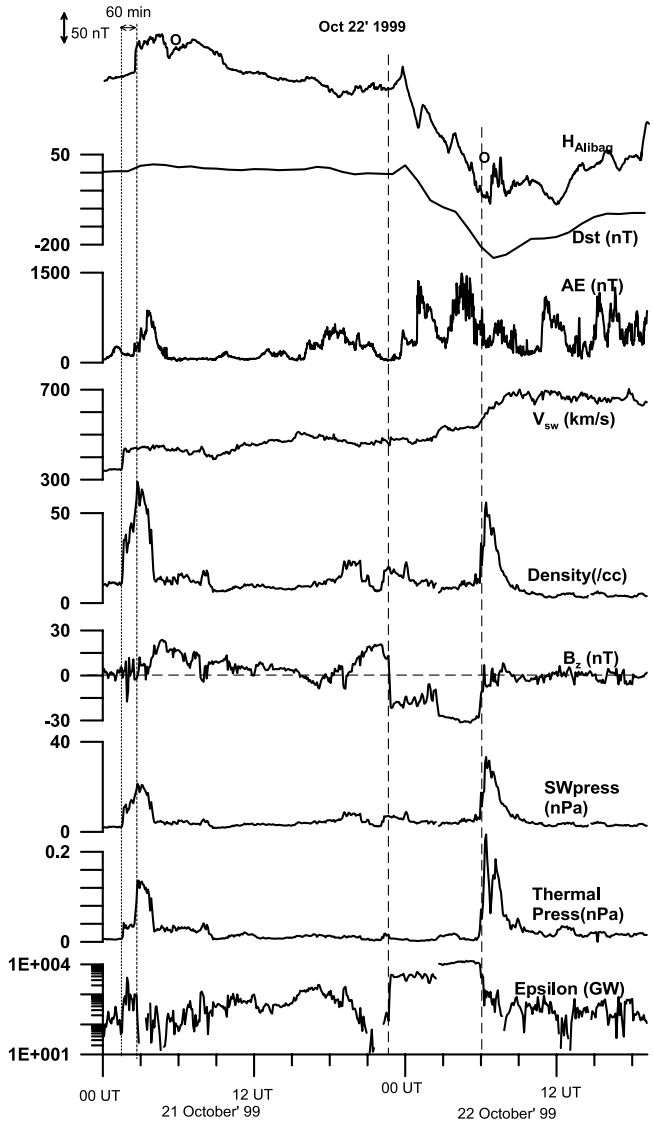

Figure 2. Observed and derived solar wind parameters during 21–22 October 1999.

[20] High-density impulse at 0130 UT on 21 October 1999, accompanied by sudden increase in the solar wind velocity obviously indicates the occurrence of shock, which results in the SSC observed on the ground after the time lag of ~60 min (vertical dotted lines on the left side of the figure). The open circle shows the local noon at Alibag. Normally, SSC marks the beginning of the initial phase of the storm. However, there are evidences of ring current enhancement without the occurrence of SSC [*Hirshberg*, 1963]. In addition, *Akasofu* [1964] showed that SSCs are not always followed by storm main phases or auroral

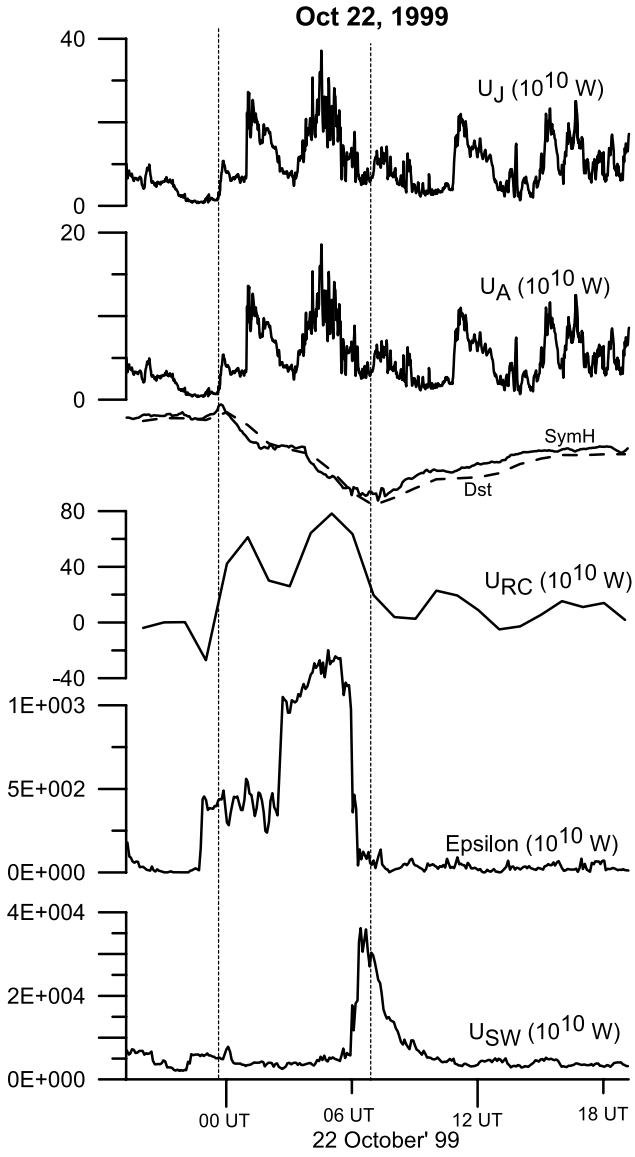

Figure 3. Temporal variation of solar wind and magnetospheric energetics during the storm on 22 October 1999.

activity. In the present case we do observe the development of ring current but almost 22 hours after the occurrence of SSC. Therefore the question is whether one should consider the case of elongated initial phase or something else? *Tsurutani et al.* [1988] have reported that peak southward IMF events occurred within 36 hours after the onset of the interplanetary disturbance, using the observations for the year 1978–1979, out of which majority occurred within 10–20 hours. In this context it is useful to inspect the activity during this period. The B_z component of IMF was directed northward till the start of main phase interval. The plasma density immediately dropped down after the initial density enhancement that lasted for ~3 hours and subsequently remained relatively low till 0600 UT of 22 October. One can see that small southward turning of the IMF also results in the transfer of energy. IMF turned southward at 2300 UT on 21 October and remained southward for next 8 hours (interval marked by vertical dashed lines), reaching its maximum value of 31.5 nT. The coupling function reaches its maximum value of 1.3×10^{13} Watt, corresponding to the largest southward turning of IMF.

[21] During the main phase interval, multiple peak structures are observed in the horizontal magnetic field component recorded at the low-latitude station (see the top panel of Figure 2) and in the *AE* index. Clear impact of the density hike at 0600 UT on 22 October is seen in the low-latitude (Alibag) magnetic field after 1 hour. The solar wind pressure increases from 4 nPa to 33 nPa, due to this high-density pulse. Small increase in *AE* index at 1800 UT on 21 October could find a cause in the southward fluctuation of IMF of very small duration. It is seen from Figure 2 that the enhanced auroral activity is always accompanied by some fluctuations in the IMF. Alibag magnetic field record also shows these fluctuations, however the *Dst* index does not always reflect these small-scale IMF variations. Since *Dst* has time resolution of 1 hour, we have plotted 1-min values of *SymH* index in Figure 3, which is basically the same as *Dst* except the time resolution (Other parameters shown in this figure are discussed in the next subsection). We observe that even higher resolution values of ring current index do not always show the signatures of small fluctuations in the interplanetary magnetic field.

[22] In order to inspect the cause of this storm, in conjunction with other parameters, we have plotted temperature of the solar wind and magnitude of IMF, along with all the three components in Figure 4. It is seen that the magnetic field, *B*, is strong, and the density and temperature are somewhat low, until 0600 UT on 22 October. This may

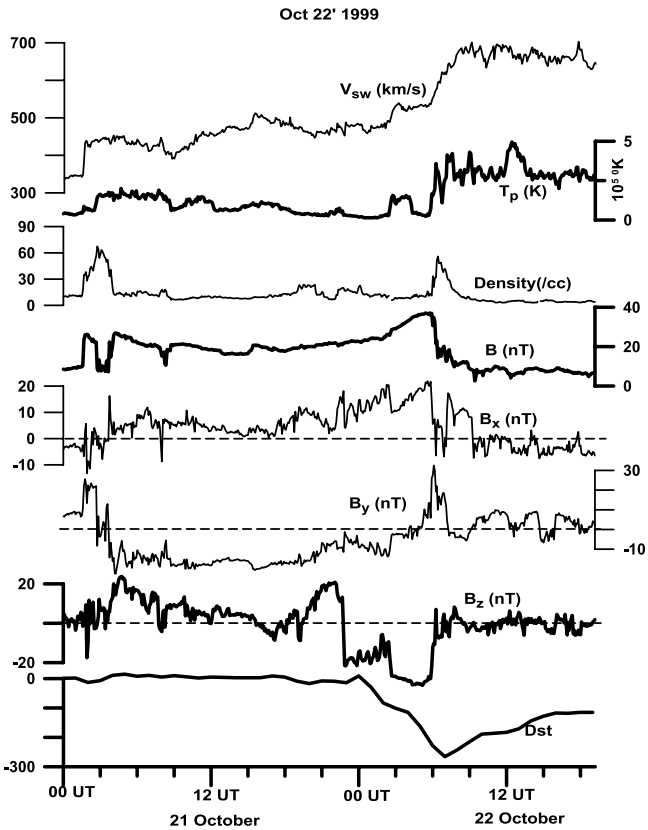

Figure 4. Solar wind parameters along with Dst on 22 October 1998.

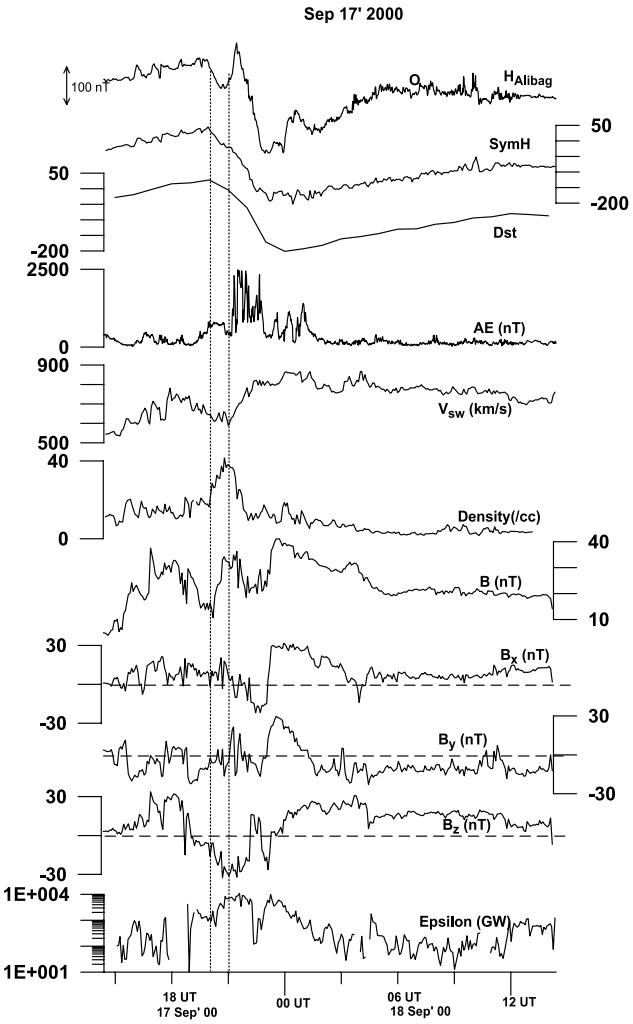

Figure 5. Variations of geophysical parameters for the magnetic storm on 17–18 September 2000.

indicate the presence of magnetic cloud (for magnetic cloud signature, please refer to section 5). However, later on, magnetic field drops to lower values and proton temperature attains higher values; a sudden increase in solar wind density and velocity is also observed. The southward component of IMF does not show smooth turning to northward direction. These signatures do not hold up magnetic cloud structure. Hence we remark an unusual event for the present storm.

[23] The temporal variation of energy rates in various regions of the magnetosphere is plotted in Figure 3. *Dst* index is shown by dashed curve, whereas solid curve indicates one-minute values of *SymH* variations. We have marked the main phase interval by dotted vertical lines, based on *Dst* variations. The auroral activity is also high during this interval.

[24] The estimates of $U_{SW,}$ epsilon, U_J, U_A, and U_{RC} are computed using equations (2), (3), (6), (7), and (8), respectively. We find that the kinetic power of the solar wind is one order of magnitude larger than epsilon during the course of the storm period. However, the kinetic energy flux profile shows no temporal correlation with the storm energy dissipation in the magnetosphere-ionosphere system. The plots show a time lag of 1 hour between magnetospheric coupling function (ε) and ionospheric dissipated energies. The ring current energy injection rate is high during the main phase interval with double peak structure. During recovery phase, the ε function drops drastically but the auroral dissipation (both U_J and U_A) is still high. For the total storm period, around 4.5% of the total solar wind energy gets coupled with the magnetosphere and 15.5% of magnetospheric energy gets dissipated into the auroral ionosphere and ring current. The energy injected in the course of the main phase into the inner magnetosphere and ionosphere of both hemispheres amounts to 1.3% of the solar wind kinetic energy and the percentage reduces to 0.75 during recovery phase.

4.2. The 17–18 September 2000 Storm

[25] During the magnetic storm of 17–18 September 2000, the low-latitude magnetic measurements showed disturbed variations before the onset of the main phase, and hence it was not possible to identify the occurrence of SSC clearly. The *Ap* index before the occurrence of storm was very high; the consecutive *Ap* values for previous 3 days were 12, 29, and 56. During the main phase interval of the storm (see Figure 5), the plasma density increases from 10/cc to 40/cc (interval enclosed by the vertical dotted lines). This high-density pulse with southward IMF shows signature at low-latitude ground magnetic observatory and in the auroral activity index as well. The enhanced *AE* activity between 2200 UT on 17 September and 0100 UT on 18 September are associated with the southward turning of the IMF and also with the increased solar wind densities. Alibag magnetic field record with 1-min time resolution indicates some fluctuations during this time, but hourly values of *Dst* index show smooth variation. In order to examine the higher-frequency variations of *Dst*, we have also shown *SymH* variations of 1-min resolution in Figure 5, which contain some fluctuations but fail to bring out the signature of large solar wind density during the main phase.

[26] Further, it should be noted that the storm main phase commences in near coincidence (delay ~1 hour) with the southward turning of the IMF. It remains southward until 2220 UT, during which it reaches maximum of 33 nT. Then after retaining northward direction for small duration, IMF again turns southward at 2245 UT, keeping the same orientation till 2335 UT on 17 September 2000, during which southward IMF reaches the magnitude of ~27 nT. Hence the main phase extends further beyond 2400 UT. The strength of the interplanetary magnetic field is high during this time. The magnetospheric coupling function increases to 1.0×10^{13} Watt.

5. Magnetic Clouds

[27] During solar maximum, the Sun's activity mostly includes flares, coronal mass ejections (CMEs), etc., and the intense magnetic storms can find origin in it. Particularly, a distinct class of solar ejecta, which is interplanetary manifestations of fast CMEs, known as magnetic cloud structures, are found to be responsible to significant extent for the occurrence of intense geomagnetic storms [*Tsurutani et al.*, 1992; *Burlaga et al.*, 1981; *Klein and Burlaga*, 1982].

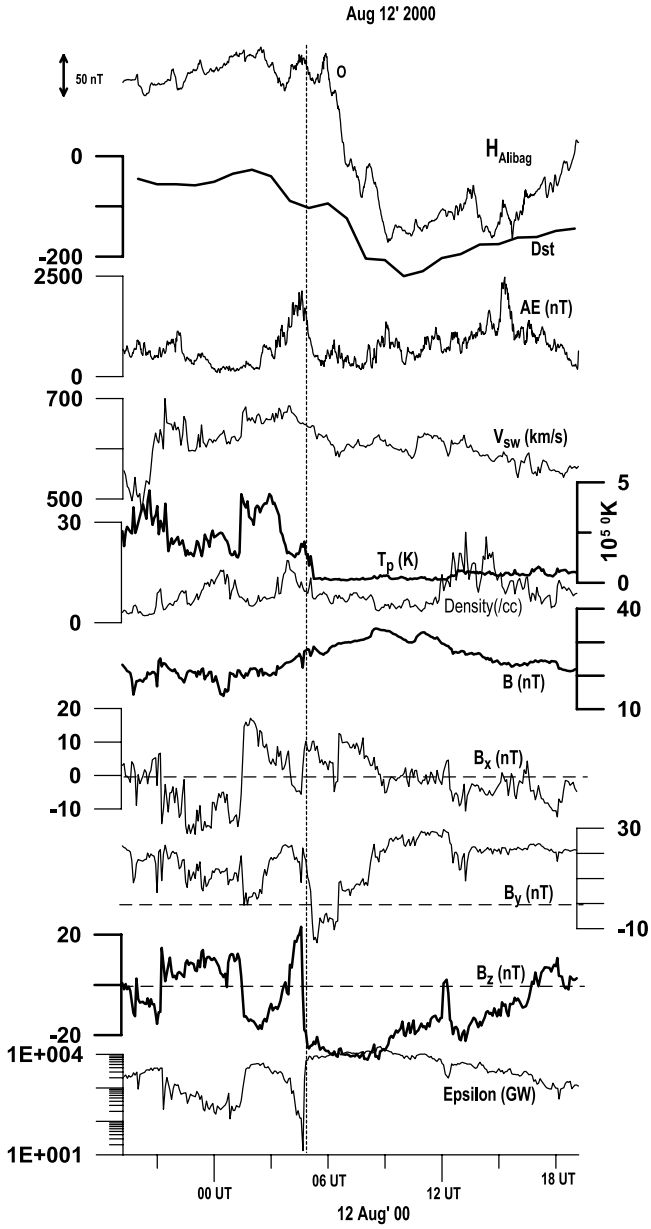

Figure 6. Magnetic cloud: Variation of solar wind parameters and indices on 12 August 2000.

[28] Magnetic cloud event is characterized by (1) enhanced magnetic field strengths, (2) a large and smooth rotation of the magnetic field vector, and (3) low proton temperatures. Magnetic clouds lead to magnetic storms during southward magnetic field portion of the cloud. Various properties of the magnetic clouds such as its global topology, temporal evolution, boundaries, effects on magnetosheath, ionosphere, nightside magnetosphere, etc., have been reviewed extensively by *Farrugia et al.* [1998].

[29] Here, we present one storm event that took place in the year 2000 that is a year of maximum solar activity (average sunspot number ~120). Figure 6 shows magnetic cloud starting just after 0430 UT on 12 August 2000 (shown by dashed vertical line). Note that the southward turning of the IMF is abrupt and it remains almost constant for ~4 hours and then the field slowly and smoothly rotates to northward direction, except for the fluctuation of small duration at 1200 UT. The strength of IMF is high (~30 nT), with low plasma temperature. The recovery starts as the field becomes less southward.

[30] Note that the AE activity is high during southward turning of the IMF and it is further enhanced due to the higher solar wind density. This is because of the southward IMF that allows the high-density solar wind particles to enter into the auroral ionosphere. Again, the signature of high solar wind density impulse at ~1400 UT is seen in the *AE* index. The horizontal magnetic field variations at Alibag observatory and *SymH* index (see Figure 7) show some fluctuations corresponding to this solar wind density increase. The epsilon function shows higher magnitude during the period of southward IMF.

[31] The energy profiles during this event are shown in Figure 7. The storm main phase duration is marked by dashed vertical lines. Note from the figure that the solar wind kinetic energy correlate well with the dissipation energy in auroral ionosphere. Since the IMF is southward for most of the time shown in figure, the conditions are

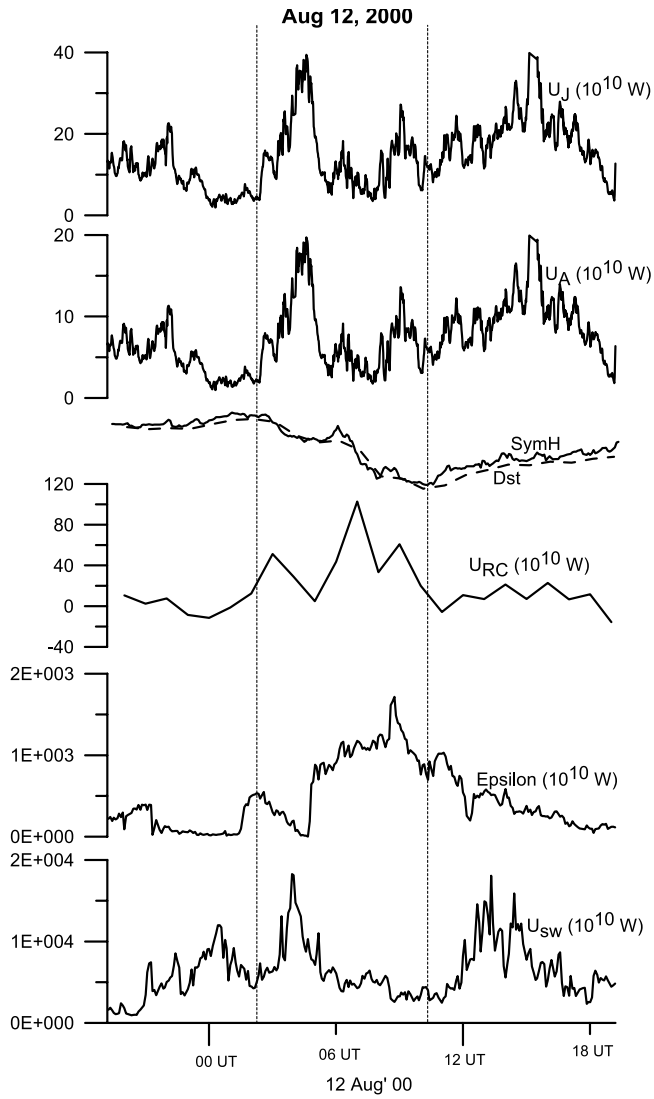

Figure 7. Temporal variation of storm energetics during the storm on 12 August 2000.

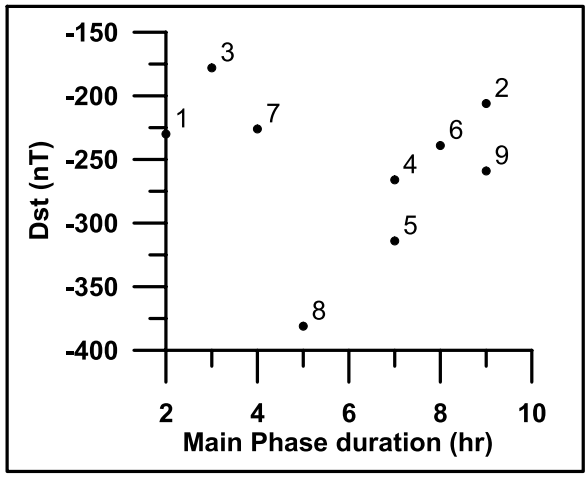

Figure 8. Scatterplot of maximum deviation of *Dst* verses main phase duration.

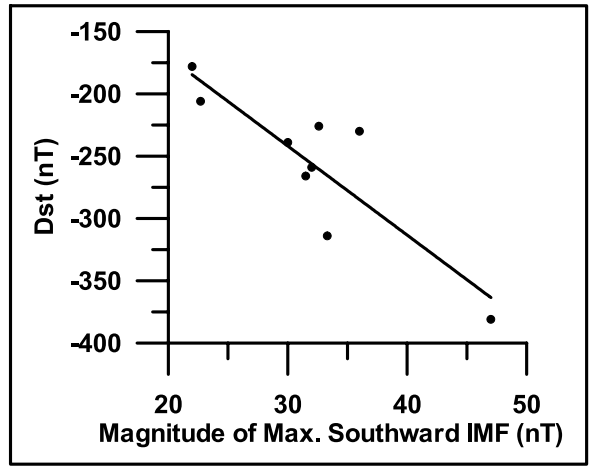

Figure 10. Scatterplot of maximum deviation of *Dst* verses maximum southward IMF.

favorable for the coupling of the solar wind and magnetosphere. Then, the next enhancing factor for auroral activity is solar wind density. Thus the auroral activity enhancement results due to combined effect of southward turning of IMF and increased solar wind density.

[32] The ring current injection rate does not indicate any significant injections, for the increase in the solar wind density with southward IMF after 1200 UT. The correlation of storm time ring current injection is better with magnetospheric coupling (and hence with southward component of IMF) than with the solar wind kinetic energy. The ring current injection rate indicates multipeak structure during the main phase of the storm.

6. Results and Discussion

6.1. Dependence of Main Phase Interval

[33] Numerous case and statistical studies have verified the relationship between strength of the storm and the main phase duration [*Yokoyama and Kamide*, 1997], but to date, it has not been adequately quantified. In order to study the relationship between the intensity of the magnetic storms and the main phase interval, we have plotted maximum *Dst* deviation verses main phase duration in Figure 8. The plot shows a large scatter. Further, in order to get some more information, we have labeled each point by the serial number of the event shown in Table 1. The magnetic cloud events (labeled by 2, 4(?), 5, 6, 9) lie on the right-hand side and indicate inverse proportionality of *Dst* deviation with the main phase duration, which is not in agreement with the earlier statistical study by *Yokoyama and Kamide* [1997] for the period between 1983 and 1991. It should be noted that they have covered almost one solar cycle, whereas our study is mainly near solar maximum. This could raise some questions such as, does the distinct class of magnetic cloud events studied here responsible for this discrepancy, or does the difference in solar activity for the two studies lead to the contradiction? Furthermore, our study is individual storm-based, whereas the analysis of *Yokoyama and Kamide* [1997] considers the average values of *Dst* index for different categories of magnetic storms. Evidently, further studies involving large number of intense magnetic storms that analyze the storm statistics separately for magnetic cloud events and various solar activity levels are needed to answer the above queries. However, we observe from Figure 9 that the variation of the main phase interval with the duration of the southward IMF shows less scatter leading to better linear dependence.

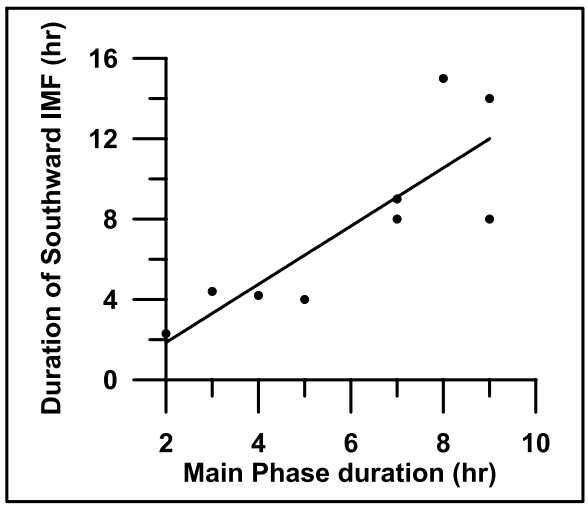

Figure 9. Variation of the duration of southward IMF verses main phase duration.

[34] The plot of maximum deviation of *Dst* verses magnitude of maximum southward IMF as shown in Figure 10

Table 2. Energy Budget During Main Phase of the Storm[a]

Event	E_{SW}	E_J	E_A	E_{RC}	E_M	$E_T = E_J + E_A + E_{RC}$
4 May 98	1986	1.8	0.9	7.7	72	10.5
25 Sep 98	2390	5.3	2.6	14.1	147	22.0
22 Sep 99	874	1.4	0.7	8.2	24	10.2
22 Oct 99	1946	3.5	1.7	14.8	182	20.0
6 Apr 00	3825	3.8	1.9	18	165	23.7
12 Aug 00	1858	4.6	2.3	13.6	232	20.5
17 Sep 00	3231	2.7	1.4	11.1	67	15.2
31 Mar 01	3871	2.3	1.1	19.2	201	22.6
11 Apr 01	7201	5.8	2.9	15.0	159	23.7
Average	3020	3.5	1.7	13.5	139	18.7

[a]Energies are expressed in 10^{15} J.

Table 3. Energy Budget for Total Storm Period[a]

Event	E_{SW}	E_J	E_A	$E_I = E_J + E_A$	E_{RC}	E_M	$E_T = E_I + E_{RC}$
4 May 98	8490	9.3	4.6	13.9	15.5	177	29.4
25 Sep 98	4548	14.4	7.2	21.6	15.8	261	37.4
22 Sep 99	5131	5.0	2.5	7.5	14.1	73	21.7
22 Oct 99	4781	8.8	4.4	13.3	19.9	215	33.2
6 Apr 00	7488	6.7	3.34	10.0	25.1	193	35.1
12 Aug 00	5464	12.4	6.2	18.6	19.0	382	37.6
17 Sep 00	12440	6.1	3.0	9.1	16.5	95	25.6
31 Mar 01	13752	12.7	6.4	19.1	40.0	562	59.0
11 Apr 01	8780	10.6	5.31	15.9	20.4	272	36.3
Average	7874.9	9.6	4.8	14.3	20.7	248	35.0

[a]Energies are expressed in 10^{15} J.

clearly shows linear relationship between these two. Hence present study indicates that the strength of the magnetic storm is directly proportional to the strength of southward IMF.

6.2. Energy Budget of Intense Storms

[35] Using the expressions for energy rates given in section 3, we have computed various components of magnetospheric and ionospheric energies involved during the occurrence of storm. The energies in the units of Joules are obtained through time integration of the energy rates. In order to estimate the total energy input to the magnetosphere (E_M), we have used epsilon parameter. Table 2 indicates the energy budget during main phase of the storm. E_{SW} denotes total kinetic energy of solar wind, whereas ionospheric dissipated energies due to joule heating, auroral particle precipitation, and ring current are denoted by E_J, E_A, and E_{RC}, respectively. E_T indicates total energy dissipated. Note that the quantities E_J and E_A are for one hemisphere only.

[36] During the main phase of the storm, the energy available in the solar wind ranges from 9×10^{17} to 72×10^{17}J and the average is 30×10^{17}J. Earlier study by *MacMahon and Gonzalez* [1997] has reported an average value of 65×10^{17} J for the solar wind energies for the four storms taking place between 1980 and 1982, whereas study by *Feldstein et al.* [2003] estimates the solar wind kinetic energy equal to $20-50 \times 10^{17}$ J. Thus the present estimates are in good agreement with the earlier investigations. It should be noted that for the computation of solar wind kinetic energy, we consider the magnetosphere scale length for the effective cross section to be equal to a constant value of 30 R_E [*Weiss et al.*, 1992], which could lead to considerable residual uncertainties in the estimates of E_{SW}, whereas computation of magnetosphere coupling energy takes into account the movement of the dayside magnetopause, and hence the uncertainties involved are not significant. The mean of the energy transferred into the magnetosphere comes to $\sim 140 \times 10^{15}$ J. The energy dissipated in the auroral ionosphere and through Joule heating varies between 2×10^{15} and 9×10^{15} J. Ring current energies range from 8×10^{15} to 19×10^{15} J, with an average of 13.5×10^{15} J. About 5% of total solar wind kinetic energy is available for the redistribution in the magnetosphere during main phase. Whereas around 13.5% of magnetospheric energy goes into the auroral dissipation, Joule heating (one hemisphere), and ring current, the estimation turns to 18% by considering the energy dissipated in both the hemispheres. It is also noted that less than a percent of solar wind kinetic energy gets dissipated into the auroral ionosphere and ring current system, which is in accordance with the results obtained by *MacMahon and Gonzalez* [1997]. Since the expressions for Joule heating and auroral particle precipitation are only for one hemisphere, in order to account for both the hemispheres, we have doubled the estimates, assuming that the energy dissipation in both the hemispheres is same. The comparison of the energy estimates from various previous studies have been done by *Feldstein et al.* [2003], and it is found that they are pretty contradictory to each other.

[37] Table 3 represents the energy budget for the total storm period. The duration of the total period of the magnetic storm varies from one storm to another; basically it consists of three phases: (1) prior to main phase, (2) main phase, and (3) recovery phase. The duration of the first phase ($\leq$5 hours) is determined by the inspection of various energy rates, especially epsilon parameter. On an average the total period of the storm is $\sim$24 hours; the duration is 36 hours for the storm on 31 March 2001. It should be noted that in the present study, we consider the recovery phase ends at the time when the derivative of *Dst* is significantly small, rather than when *Dst* reaches exactly to its prestorm value.

[38] It would be interesting to study the energetics involved in the storm main phase and recovery phase separately. Therefore we propose Table 4, which shows the percentage of (E_M/E_{SW}) during total storm period, main phase, and recovery phase separately. The table depicts that the ratio of the energy available for the redistribution in the magnetosphere to the total solar wind kinetic energy is always higher during main phase than during recovery phase, with one exception of storm on 11 April 2001. For this event, the percentage is fairly higher in the recovery phase, which is due to relatively very low value of E_{SW} during the recovery phase. On an average, during main

Table 4. Percentage Rate Between Energy Transferred to the Magnetosphere and Solar Wind Kinetic Energy

	(E_M/E_{SW})%		
Event	Total	Main	Recovery
4 May 98	2.1	3.6	1.6
25 Sep 98	5.8	6.2	5.3
22 Sep 99	1.4	2.8	1.1
22 Oct 99	4.5	9.4	1.2
6 Apr 00	2.6	4.3	0.8
12 Aug 00	7.0	12.5	4.2
17 Sep 00	0.8	2.1	0.3
31 Mar 01	4.1	5.2	3.7
11 Apr 01	3.1	2.2	7.2
Average	3.2	4.6	2.3

phase of the storm, almost 5% of the total solar wind kinetic energy is available for the redistribution in the magnetosphere, whereas during recovery phase it reduces to 2.3%.

[39] For the total storm period (Table 3), the energy dissipated through the particle precipitation in the auroral ionosphere varies from 3×10^{15} to 7×10^{15} J, whereas that for Joule heating ranges from 5×10^{15} to 14×10^{15} J. Ring current energy estimates vary between 14×10^{15} and 40×10^{15} J, with an average of 21×10^{15} J. About 3.5% of E_{SW} is available for the redistribution in the magnetosphere and around 20% of E_M goes into total magnetospheric energy consumption in both the hemispheres. The differences between E_M and E_T could be attributed to the energy consumption in the magnetospheric tail current and the field-aligned current. Wide range of energies stored in various parts of the magnetosphere indicates that though all the storms fall in the same category of "intense storms," each event involves different energy budget. This further suggests that the nature of the magnetospheric response during storm time depends on the conditions of solar ejecta substantially.

7. Summary

[40] All nine cases confirm the crucial role of southward component of IMF (B_Z) in the development of the geomagnetic storm. Though the general dependence of storm intensity (*Dst*) on the strength and the duration of the southward IMF is not yet found, *Gonzalez and Tsurutani* [1987] have suggested threshold values of southward IMF (magnitude $\geq$10 nT and duration $\geq$3 hours) for intense storms with $|Dst| \geq 100$ nT. The present investigation reveals that the strength of ring current (*Dst* deviation) depends on the magnitude of southward IMF, in agreement with the above threshold value provided by *Gonzalez and Tsurutani* [1987]. The dependence of the duration of main phase on the strength of the storm is not clear. However, the main phase duration shows clear dependence on the duration of southward IMF.

[41] We find that the kinetic power of the solar wind is one to two orders of magnitude larger than epsilon function during the course of the storm period. The temporal variation of the storm energy injection in ring current correlates well with the epsilon parameter and hence with the southward component of IMF. Multiple peak structure in the ring current energy injection rate is observed during longer main phase intervals with multiple southward turnings of IMF.

[42] It is observed from the entire storm events studied here that the enhanced auroral activity is always associated with the southward turning of the IMF, even weak and fluctuating component of southward IMF results in the enhancement of *AE* index. On the other hand, *Dst* or *SymH* do not have significant influence of fluctuating southward IMF. This is in accordance with the study by *Kamide* [2001]. Further, we observe that having southward IMF, auroral activity is next controlled by the kinetic energy of the solar wind (Figures 6 and 7). Therefore the substorm activity deduced from *AE* index is found to emerge primarily due to the southward component of IMF and secondarily due to the solar wind kinetic energy flux profile. Thus the present investigation confirms that both the substorm activity and the ring current development are mainly controlled by the southward turning of the IMF.

[43] Using *ASY-D*, *ASY-H*, and *AL* indices and Pi2 geomagnetic pulsations for the detection of the onset of the substorm activity, *Iyemori and Rao* [1996] have found no statistically significant development in the *Dst* index after the onset of substorms. We also find poor correlation between auroral activity and *Dst* or *SymH* variations. Thus the present study supports the above finding by *Iyemori and Rao* [1996]. Besides this we also observe that 1-min measurements of the horizontal magnetic field at Alibag appear to have some signatures of southward turning of the IMF of short duration and of the enhancement in solar wind density (refer to Figure 2). This suggests that the integrated study with the low-latitude magnetic field variations during major storms could provide better insight into the understanding of the electrodynamics associated with the high-latitude–low-latitude coupling.

[44] The location of the subsolar point is found to be sensitive to the solar wind density changes. Hence we have computed the epsilon parameter by taking into account the variation in the size of the magnetosphere. We find that the epsilon parameter is well above the typical storm threshold values of 10^{12} W [*Akasofu*, 1981b] in all cases under study. Present investigation reveals that from the energy available in the magnetosphere, around 20% is distributed in the ring current and auroral ionosphere during main phase of the storm, which is much below than that reported by *MacMahon and Gonzalez* [1997] and *Knipp et al.* [1998]. The present investigation suggests that less than a percent of solar wind kinetic energy dissipates into the auroral ionosphere and ring current system, which is in accordance with the results obtained by *MacMahon and Gonzalez* [1997]. Note that in the present study, we do not compute the energy of magnetospheric tail current and the energy delivered to the magnetosphere through the generation of field-aligned currents. Additionally, the *AE* indices are based only on latitudes greater than 60°; hence there is a possibility of underestimation of those indices and hence our calculations of the auroral and Joule heat dissipation rates are probably an underestimation during the early part of the main phase. Around 5% of the total solar wind kinetic energy is available for the redistribution in the magnetosphere during main phase of the storm, whereas during total storm period and recovery phase, the percentage becomes 3.5% and 2.3%, respectively.

[45] **Acknowledgments.** The authors are grateful to NSSDC at NASA Goddard Space Flight Center for making available the ACE satellite measurements. We thank the ACE SWEPAM instrument team, ACE Magnetic Field instrument team, and the ACE Science Center for providing the ACE data. We are also thankful to WDC-C2, Kyoto, for supplying *Dst* and SymH indices. Some portions of the work were done while G. S. Lakhina was visiting Solar Terrestrial Environment Laboratory (STEL), Nagoya University, Toyokawa, Japan. He would like to thank Y. Kamide for the kind hospitality. We are grateful to the reviewers for their insightful and revealing comments, which have helped to clarify some of the explanations in the manuscript.

[46] Lou-Chuang Lee thanks Walter Gonzalez and Bruce Tsurutani for their assistance in evaluating this paper.

References

Akasofu, S. I. (1964), A source of the energy for geomagnetic storms and auroras, *Planet. Space Sci.*, *12*, 801.

Akasofu, S. I. (1981a), Energy coupling between the solar wind and the magnetosphere, *Space Sci. Rev.*, *28*, 121.
Akasofu, S. I. (1981b), Relationship between AE and Dst indices during geomagnetic storms, *J. Geophys. Res.*, *86*, 4820.
Akasofu, S. I., and S. Chapman (1961), The ring current geomagnetic disturbances and Van Allen radiation belts, *J. Geophys. Res.*, *66*, 1321.
Alexeev, I. I., and Y. I. Feldstein (2001), Modeling of geomagnetic field during magnetic storms and comparison with observations, *J. Atmos. Sol. Terr. Phys.*, *63*, 431.
Baker, D. N., N. E. Turner, and T. I. Pulkkinen (2001), Energy transport and dissipation in the magnetosphere during geomagnetic storms, *J. Atmos. Sol. Terr. Phys.*, *63*, 421.
Baumjohann, W., and Y. Kamide (1984), Hemispherical Joule heating and the AE indices, *J. Geophys. Res.*, *89*, 383.
Burlaga, L. F., E. Sittler, F. Mariani, and R. Schwenn (1981), Magnetic loop behind an interplanetary shock: Voyager, Helios and IMF-8 observations, *J. Geophys. Res.*, *86*, 6673.
Burton, R. K., R. L. McPherron, and C. T. Russell (1975), An empirical relationship between interplanetary conditions and *Dst*, *J. Geophys. Res.*, *80*, 4204.
Chapman, S. (1962), Earth storms: Retrospect and prospect, *J. Phys. Soc. Jpn.*, *17*, suppl. A-I, 6.
Dessler, A. J., and E. N. Parker (1959), Hydromagnetic theory of magnetic storms, *J. Geophys. Res.*, *64*, 2239.
Ebihara, Y., and M. Ejiri (2000), Simulation study on fundamental properties of the storm-time ring current, *J. Geophys. Res.*, *105*, 15,843.
Farrugia, C. J., L. F. Burlaga, and R. P. Lepping (1998), Magnetic clouds and the quiet-storm effect at Earth, in *Magnetic Storms*, *Geophys. Monogr. Ser.*, vol. 98, edited by B. T. Tsurutani et al., pp. 91–106, AGU, Washington, D. C.
Feldstein, Y. I. (1992), Modeling of the magnetic field of magnetospheric ring current as a function of interplanetary medium parameters, *Space. Sci. Rev.*, *59*, 83.
Feldstein, Y. I., L. A. Dremukhina, A. E. Levitin, U. Mall, I. I. Alexeev, and V. V. Kalegaev (2003), Energetics of the magnetosphere during the magnetic storm, *J. Atmos. Sol. Terr. Phys.*, *65*, 429.
Garrett, H. B., A. J. Hassler, and T. W. Hill (1974), Influence of solar wind variability on geomagnetic activity, *J. Geophys. Res.*, *79*, 4603.
Gonzalez, W. D., and B. T. Tsurutani (1987), Criteria of interplanetary parameters causing intense magnetic storms (*Dst* < −100 nT), *Planet. Space Sci.*, *35*, 1101.
Gonzalez, W. D., A. L. C. Gonzalez, J. H. A. Sobral, A. Dal Lago, and L. E. Vieira (2001), Solar and interplanetary causes of very intense geomagnetic storms, *J. Atmos. Sol. Terr. Phys.*, *63*, 403.
Hamilton, D. C., G. Gloeckler, F. M. Ipavich, W. Studemann, B. Wilken, and G. Kremser (1988), Ring current development during the great geomagnetic storm of February 1986, *J. Geophys. Res.*, *93*, 14,343.
Hirshberg, J. (1963), Note on ring currents in the absence of sudden commencement storms, *J. Geophys. Res.*, *68*, 6201.
Huttunen, K. E. J., H. E. J. Koskinen, T. I. Pulkkinen, A. Pulkkinen, M. Palmroth, E. G. D. Reeves, and H. J. Singer (2002), April 2000 magnetic storm: Solar wind driver and magnetospheric response, *J. Geophys. Res.*, *107*(A12), 1440, doi:10.1029/2001JA009154.
Iyemori, T., and D. R. K. Rao (1996), Decay of the Dst field of geomagnetic disturbance after substorm onset and its implication to storm-substorm relation, *Ann. Geophys.*, *14*, 608.
Jacobs, J. A. (1991), *Geomagnetism*, vol. 4, Elsevier, New York.
Joselyn, J. A., and B. T. Tsurutani (1990), Geomagnetic sudden impulses and storm sudden commencements, *Eos Trans. AGU*, *71*, 1808.
Kamide, Y. (2001), Interplanetary and magnetospheric electric fields during geomagnetic storms: what is more important, steady-state fields or fluctuating fields?, *J. Atmos. Sol. Terr. Phys.*, *63*, 4113.
Klein, L. W., and L. F. Burlaga (1982), Interplanetary magnetic clouds at 1 AU, *J. Geophys. Res.*, *87*, 613.
Knipp, D. J., et al. (1998), An overview of the early November 1993 geomagnetic storm, *J. Geophys. Res.*, *103*, 26,197.
Liemohn, M. W., J. U. Kozyra, V. K. Jordanova, G. V. Khazanov, M. F. Thomsen, and T. E. Cayton (1999), Analysis of early phase ring current recovery mechanism during geomagnetic storms, *Geophys. Res. Lett.*, *26*, 2845.
MacMahon, R. M., and W. D. Gonzalez (1997), Energetics during the main phase of geomagnetic superstorms, *J. Geophys. Res.*, *102*, 14,199.
Martyn, D. F. (1951), The theory of magnetic storms and auroras, *Nature*, *167*, 92.
Nishida, A. (1983), IMF control of the Earth's magnetosphere, *Space Sci. Rev.*, *34*, 185.
O'Brien, T. P., and R. L. McPherron (2000), An empirical phase space analysis of ring current dynamics: solar wind control of injection and decay, *J. Geophys. Res.*, *105*, 7707.
Perreault, P., and S. I. Akasofu (1978), A study of magnetic storms, *Geophys. J. R. Astron. Soc.*, *54*, 547.
Sckopke, N. (1966), A general relation between the energy of trapped particles and the disturbance field near the earth, *J. Geophys. Res.*, *71*, 3125.
Sibeck, N., R. E. Lopez, and E. C. Roelof (1991), Solar wind control of the magnetopause shape, location and motion, *J. Geophys. Res.*, *96*, 5489.
Tsurutani, B. T., and W. D. Gonzalez (1997), The interplanetary causes of magnetic storms: A review, in *Magnetic Storms*, *Geophys. Monogr. Ser.*, vol. 98, edited by B. T. Tsurutani et al., pp. 77–89, AGU, Washington, D. C.
Tsurutani, B. T., W. D. Gonzalez, F. Tang, S. I. Akasofu, and E. Smith (1988), Origin of interplanetary southward magnetic fields responsible for major magnetic storms near solar maximum (1978–1979), *J. Geophys. Res.*, *93*, 8519.
Tsurutani, B. T., W. D. Gonzalez, F. Tang, Y. T. Lee, M. Okada, and D. Park (1992), Reply to L. J. Lanzerotti: Solar wind ram pressure corrections and an estimation of the efficiency of viscous interaction, *Geophys. Res. Lett.*, *19*, 1993.
Turner, N. E., D. N. Baker, T. I. Pulkkinen, J. L. Roeder, J. F. Fennell, and V. K. Jordanova (2001), Energy content in the storm time ring current, *J. Geophys. Res.*, *106*, 19,149.
Valdivia, J. A., A. S. Sharma, and K. Papadopoulos (1996), Prediction of magnetic storms by nonlinear models, *Geophys. Res. Lett.*, *23*, 2899.
Weiss, L. A., P. H. Reiff, J. J. Moss, R. A. Heelis, and B. D. Moore (1992), Energy dissipation in substorms, in *Substorms 1, ESA SP-335*, pp. 309–317, Eur. Space Agency, Paris.
Yokoyama, N., and Y. Kamide (1997), Statistical nature of geomagnetic storms, *J. Geophys. Res.*, *102*, 14,215.

S. Alex, G. S. Lakhina, and G. Vichare, Indian Institute of Geomagnetism, Plot 5, Sector 18, New Panvel, Navi Mumbai 410 206, India. (geeta@iigs.iigm.res.in)